Sensitivity Gains in Chemosensing by Optical and Structural Modulation of Ordered Assembly Arrays of ZnO Nanorods

Defeng Zhu,[†] Qingguo He,[†,*] Qing Chen,[†] Yanyan Fu,[†] Chao He,[†,‡] Liqi Shi,[†,‡] Xin Meng,[†,‡] Changmin Deng,[†,‡] Huimin Cao,[†] and Jiangong Cheng[†,*]

[†]State Key Lab of Transducer Technology, Shanghai Institute of Microsystem and Information Technology, Chinese Academy of Sciences, Shanghai 200050, People's Republic of China, and [‡]Graduate School of Chinese Academy of Sciences, Beijing 100049, People's Republic of China

ABSTRACT Nanomaterials and -structures have attracted much attention owing to their applications to ultrasensitive nanodevices. In this work, ordered assembly arrays of ZnO nanorods have been hydrothermally fabricated and used as optical substrates of fluorescence sensors for toxic vapors. The unique fastigiate nanorod assembly combines merits of single fibers and clusters, possessing identical orientation, large surface-to-volume ratio, evanescent transmission, and evanescent coupling. As coated on the assembly arrays, different sensing materials all generated amplified spontaneous emission (ASE) action such that the fluorescence intensity of the narrowed spectrum was 52.4-fold enhanced. Results of sensing experiments indicate that sensors based on the assembly arrays displayed 100% elevated normalized quenching rate and several times longer full-load time compared with reference sensors. This work provides a facile method to fabricate secondary structures of 1D rigid material and presents a new way to design highly sensitive optic sensors. Furthermore, evanescent excitation caused ASE action of fluorescent organics, and the correlative sensitivity gain is of interest in both theoretical research and the applications field.

KEYWORDS: assembly · evanescent wave · ZnO nanorod · AFAs · fluorescence · sensor · vapor

Societal needs for greater security require dramatic improvements in the sensitivity of chemical and biological sensors. For trace vapor detection, fluorescence-based sensing has long been considered as a new-generation technique of high sensitivity and quick response.[1,2] To achieve ultrahigh sensitivity, increasing emphasis in analytical science has been directed toward materials[3−6] and devices with high nonlinear characteristics. Organic fluorescent materials[7,8] possessing amplifying nature as well as structures allowing reduction in energy threshold (E_{TH}) of amplified spontaneous emission (ASE) have been focused on.[9] Uniform array of 1D subwavelength nanofibers is proposed to significantly enhance the sensing performance of optical substrates. This should be attributed to identical orientation and large surface of the nanofibers, the evanescent-waveguiding property of a single fiber,[10,11] and spatial resonance of the array,[12] which could excite the fluorescence cladding more effectively. It was reported that the hybrid structure based on vertical ZnO nanorod arrays can simultaneously improve many critical sensing parameters in poly(phenylene ethynylene) (PPE) vapor sensing, including fluorescence intensity, quenching rate, stability, and full-load time.[13] According to the field distribution of a single nanofiber,[14] the coupled-mode theory,[15,16] and superposition principle of waves,[17] a cluster of nanofibers should provide much larger energy density on its near surface due to the stronger evanescent coupling of neighbor nanofibers. Inspired by this, a secondary architecture composed of 1D nanofibers and a 3D cluster structure is expected to further optimize the sensing properties, because it combines the merits of identical orientation, large surface-to-volume ratio, evanescent excitation, and evanescent coupling (Scheme 1). Although macroscopic fiber clusters are ubiquitous in nature, it is a great challenge to control the fabrication of such nanostructures in a reliable and cost-efficient manner.[18−20] For high-aspect ratio 1D nanofibers, a powerful approach is using a solution system,[21] but lateral adhesion occurs as an unwanted outcome, leading to uncontrolled cluster structures. The cluster features induce irregular sizes and disorder over a large area,[22] which will seriously weaken the optical modulation capacity of 1D nanostructures and limit their applications. Furthermore, flexible chain polymers, such as polyethylene glycol and polyacrylamide, have been introduced

* Address correspondence to hqg@mail.sim.ac.cn, jgcheng@mail.sim.ac.cn.

Received for review June 28, 2010 and accepted May 23, 2011.

Published online May 23, 2011
10.1021/nn103211d

in precursor solutions as 3D soft templates to regulate the morphologies of the 1D nanostructures.[23] However, the great mass of as-prepared powder samples met problems in applications because their randomness in size and shape results in poor stability and repeatability.

In this paper, ZnO nanorods were chosen as the optical nanofibers because of their wide band gap, excellent chemical and thermal stability, specific optoelectronic property, and facile fabrication processes.[24−28] The ordered arrays of fastigiate assembles (AFAs) of ZnO nanorods were successfully rooted on quartz plates and served as optical substrates of vapor sensors. Here, the special structure was hydrothermally grown with the help of a soft template, and detailed mechanisms are discussed. Using ZnO AFAs as waveguides, fluorescent materials display obvious ASE action under the excitation of low pump energy. The sensory responses show that sensitivities (fluorescence-quenching rates) and full-load times (denoting how long the sensor was responsive to the vapor) of ZnO AFA-based sensors were considerably improved compared with those of sensors based on vertical ZnO nanorod arrays or quartz plates.

RESULTS AND DISCUSSION

The tilted scanning electron microscopy (SEM) images shown in Figure 1a−d demonstrate morphologies of ZnO nanorod arrays grown for 5−8 h. Compared with vertical ZnO nanorods grown with ethanol (inset of Figure 1a), orientations of polyvinyl alcohol (PVA)-regulated ZnO nanorods were disordered at the initial stage (Figure 1a). However, a critical change appeared after about 6 h of growth, where top ends of adjacent nanorods clustered together and the whole image displayed ordered AFAs (Figure 1b). The reasons for this change are as follows. In aqueous solutions of 90 °C, free hydroxyls of PVA exhibited strong polarity and combined with functional groups (Zn−OH) on the side facets of ZnO nanorods or complexed with free Zn^{2+} in precursor solutions.[29] Simultaneously, flexible chains of PVA were coiled or stretched under magnetic stirring and thermal convection.[27] All these actions induced centripetal growth of ZnO nanorods and ultimately formed special top-assembled structures after about 6 h of growth (inset of Figure 1b), in which distances between tops were 250−300 nm and diameters of clusters were 350−400 nm. For 7 and 8 h grown AFAs, top aspects of assemblies were vertical in high uniformity (Figure 1c,d and Figure S1b, Supporting Information). The verticality of the 8 h grown AFAs was even better than that of vertical nanorod arrays reported in our previous work.[13]

The transmission electron microscopy (TEM) image of a typical ZnO nanorod in an 8 h grown assembly (Figure 1e) reveals that the growth process could be separated into five steps according to the structural

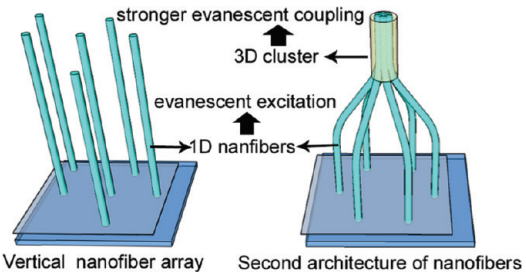

Scheme 1. Secondary architecture composed of 1D nanofibers and a 3D cluster structure.

characteristics. The novel structure, especially the reverse bend in step IV, has never been reported and was hard to interpret by conventional growth mechanisms.[30] PVA caused stresses, stiffness,[22] and lateral adhesion[31,32] of the 1D ZnO nanorod, which are proposed to be the causal factors.

A high-resolution TEM image (Figure 1f) of the selected area in Figure 1e displays a regular hexagonal crystal structure especially in straight segments. The lattice distance between adjacent lattice planes was measured as 0.5185 nm, corresponding to the *d*-spacing between (0001) planes, indicating that the ZnO nanorod was well crystallized with the *c*-axis and had a uniform optical property. This was also confirmed by the selected area electron diffraction pattern and the X-ray diffraction (XRD) pattern of the ZnO AFAs (Figure S1c, Supporting Information). Insets of Figure 1f show inverse Fourier transform images of bend areas, revealing that two kinds of crystal disfigurements, *i.e.*, edge dislocation and screw dislocation, were generated under stress to maintain the crystal growth.

The well-crystallized nature and excellent verticality of the AFAs will have important implications, especially as the array makes low-loss optical waveguiding possible. As a waveguide, the as-grown ZnO nanorod can be considered as a step-index fiber with an infinite air cladding; here the superthin fluorescent cladding is neglected. The mathematic model of this air-clad fiber is shown in Figure 2a. In fiber-optics, the critical diameter of a single-mode waveguide can be obtained from the following formula:[15]

$$V = \pi\frac{D}{\lambda_0}(n_1^2 - n_2^2)^{1/2} \leq 2.405$$

where D is the diameter of the nanorod, λ_0 is the wavelength of the excitation light, and n_1 and n_2 are the refractive indices of the core and the cladding. For the ZnO nanorod, if 400 nm excitation light is used, then λ_0 =400, n_1 = 2.03, and n_2 = 1.0, andn the critical diameter will be 176 nm, which is much larger than that of the as-grown ZnO nanorod (~45 nm) in our experiments.

By calculating exact solutions of Maxwell's equations or Helmholtz equations, the propagation constant (β) of the nanorod waveguide is obtained numerically.[33]

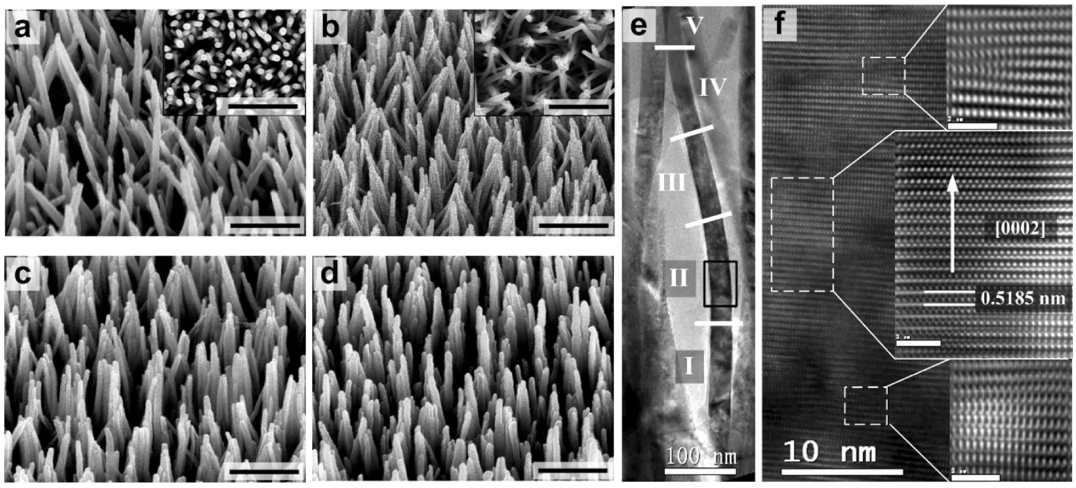

Figure 1. SEM images of ZnO AFAs grown for (a) 5 h, (b) 6 h, (c) 7 h, and (d) 8 h with 500 nm scale bars. Inset of (a) is the top-view image of ZnO nanorods grown without PVA. Inset of (b) is the top-view image of the 6 h grown AFAs. (e) TEM bright field image of a typical ZnO nanorod. (f) High-resolution TEM image of the section marked in (e). Insets are the inverse Fourier transform images of correlating areas as marked, respectively indicating edge dislocation regular lattices and screw dislocation in the ZnO crystal (from top to bottom). Scale bars in the insets are 2 nm.

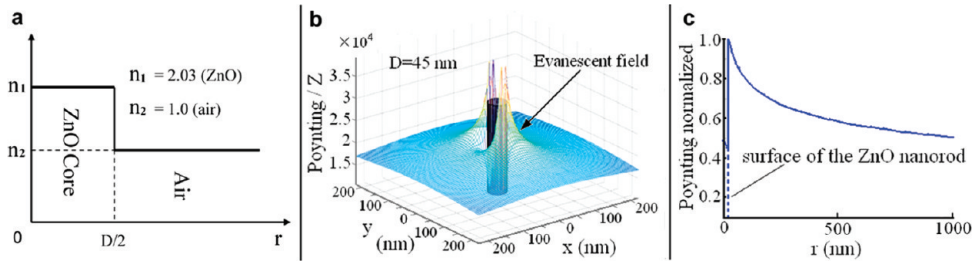

Figure 2. (a) Mathematic model of an air-clad ZnO nanorod waveguide. (b) *Z*-direction Poynting vectors (column, ZnO nanorod; gradient, field outside the nanorod) and (c) radius-dependent energy density distribution of a ZnO nanorod of 45 nm diameter, at 400 nm wavelength.

Subsequently, energy distribution can be numerically simulated upon computation of the electric and magnetic fields. In our work, we choose incident light of 400 nm wavelength, and we used excitation wavelengths of fluorescent sensing organics around 400 nm. The profile of the pointing vector for a 45 nm ZnO nanorod at 400 nm wavelength is shown in Figure 2b, in which the column stands for the nanorod and the gradient profile stands for evanescent fields. Normalized energy density as a function of the radius is shown in Figure 2c. It shows that the energy density on the surface of the nanorod is about 2 times larger than that in the center of the nanorod. In this case, we calculated that more than 90% of the incident energy was transmitted on the near surface as an evanescent wave (Figure S2, Supporting Information).

To verify the theoretical analysis, substrates listed in Table 1 were introduced as waveguides of three different sensing organics. A kind of polyfluorene (PF) derivative (inset of Figure 3) was coated on S_0–S_6 to detect diiodomethane (CH_2I_2), a typical toxic vapor in environmental pollution. Figure 3 shows fluorescence intensities at 427 nm of the sensors based on these substrates. According to the growth process, the schemes of assemblies of different growth time were outlined and pointed to corresponding intensities (original spectra see Figure S4, Supporting Information). To clearly compare the excitation capability of different substrates, intensities of reference sensors that were obtained by directly coating sensing materials on quartz plates (S_0) were 10 times magnified. Compared with reference sensors, sensors based on different kinds of ZnO nanorod arrays (S_1–S_6) possessed significantly enhanced fluorescence intensities and gradually narrowed spectra (full width at half-maximum (fwhm) of the spectra narrows from 48.1 to 41.7 nm), as shown in Figure S4, which were typical characteristics of ASE.[35] Considering preconditions of the ASE action, the net gain was higher at higher pump

TABLE 1. Optical Substrates of Sensors Used for Toxic Vapor Detection

	substrate number						
	S_0	S_1	S_2	S_3	S_4	S_5	S_6
surface structure	none	AFAs	AFAs	AFAs	AFAs	AFAs	vertical nanorod arrays
growth time	0	4 h	5 h	6 h	7 h	8 h	8 h

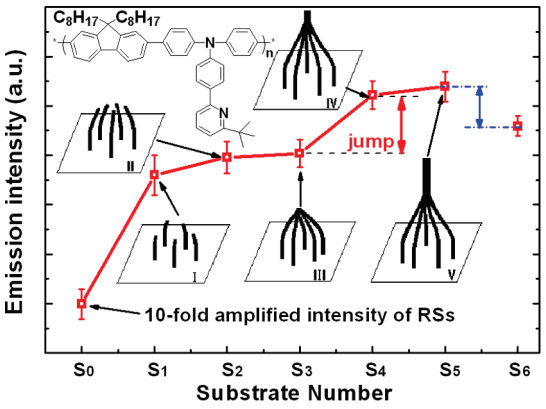

Figure 3. Emission intensity curve of the PF derivative coated sensors based on S_0−S_5. The excitation wavelength was 380 nm. Intensities of the reference sensors were 10 times amplified. Schemes outline assembly structures of different substrates, and the inset is the molecular structure of the PF derivative.

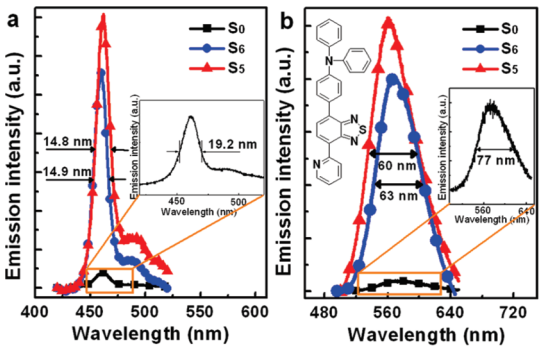

Figure 4. Fluorescence spectra of (a) PPE- and (b) TPA-BTD-Py-coated sensors based on S_0, S_5, and S_6. Inset in (c) is the molecular structure of the TPA-BTD-Py. Excitation wavelengthes for PPE and TPA-BTD-Py were 400 and 460 nm (Figure S3, Supporting Information).

intensity and the output intensity increased exponentially at vibronic peaks.[13] Thus, the phenomena should be ascribed to the evanescent excitation of ZnO nanorods, which allows higher excitation density in the fluorescent cladding. Furthermore, structural characteristics of ZnO nanorods that might reduce the threshold of ASE of the PF derivative could be another reason.[9]

Markedly, fluorescence intensities of S_5-based sensors were 52.4 times higher than those of the reference sensors. Especially, the intensity sharply jumped about 30% when S_4 was used instead of S_3. Considering morphological differences, the top section of the assembly should be responsible for the sharp increase in intensity. In the solution system, the length of the ZnO nanorod increases as growth time increases. However, the intensity increase of the sensors caused by the length increase should be slight, like that which occurs on sensors based on S_1, S_2, and S_3 (I−III in Figure 3). Therefore, we propose that the optical modulation of ZnO nanorods plays the key role in the intensity jump. Every ZnO nanorod was considered as a single-mode fiber, and the assembly of parallel nanorods should be regarded as a coupled nanofiber cluster. According to the coupled-mode theory and the superposition principle of waves,[15−17] spatial resonance of nanorod arrays can further enhance the excitation density because of evanescent-field overlapping of single ZnO nanorods.[12] Furthermore, the highly oriented nanofiber cluster could not only enhance the evanescent coupling of nanorods[10] but also couple the emission fluorescence and guide it out in an identical direction. Previous work has proved that uniform directivity of nanorod arrays affects the emission intensity seriously.[35] Slight improvement in intensities of S_4- and S_5-based sensors should also be ascribed to the length increase of the ZnO nanorods. S_6 was introduced as waveguides to test these ideas, and it brought about 42.8-fold-enhanced intensities (Figure 3, Figure S4g, Supporting Information). The layer heights of S_5 and S_6 were all about 1.25 μm, while the length of the bent nanorod was about 1.35 μm (Figure S5, Supporting Information). The diameters of the nanorods in them were almost the same (40−45 nm). The 22.3% enhancement in intensity should mainly be attributed to the structural difference (*i.e.*, the cluster) between S_5 and S_6, because the length difference was only 8%, and it slightly increased the intensity. The AFAs in S_5 possesses stronger evanescent coupling, higher excitation density, and better verticality than the vertical nanorod arrays in S_6.

To further examine the proposition, we additionally chose PPE, the polymer reported by T. M. Swager's group,[36] as the sensing material for explosive trinitrotoluene (TNT). When S_5 and S_6 were introduced as waveguides, PPE emission intensities were increased 18.2 and 13.8 times, respectively (Figure 4a). The 31.9% enhancement in intensity should also be attributed to the clusters in the AFAs. Notablely, ASE of PPE evidently occurred as S_5 and S_6 were used. The fwhm narrowed from 19.2 to 14.8 nm at the (0,0) vibrational peaks of the spectra, which was different from the result of Swager's group.[7] The result reveals that waveguides with ZnO nanorod arrays not only bring about ASE of PPE by increasing the excitation density but also effectively restrained the reabsorption losses of the (0,0) mode. When TPA-BTD-Py (inset of Figure 4b) was introduced as the third sensing material to detect the toxic aniline vapor, similar results were obtained. With the use of S_5 and S_6, the emission intensities were enhanced 25.1 and 19.7 times (Figure 4b) and the fwhm narrowed from 77 nm to 60 nm. This could strongly verify the ideas we proposed.

SEM images of ZnO AFAs display plenty of voids between ZnO nanorods, ensuring good vapor permeability for small vapor molecules. According to Fick's first law, it takes only about 10^{-5} to 10^{-4} second for vapor molecules to travel 1.25 μm to the bottom of the trench *via* the voids in the ZnO AFAs. Thus, the

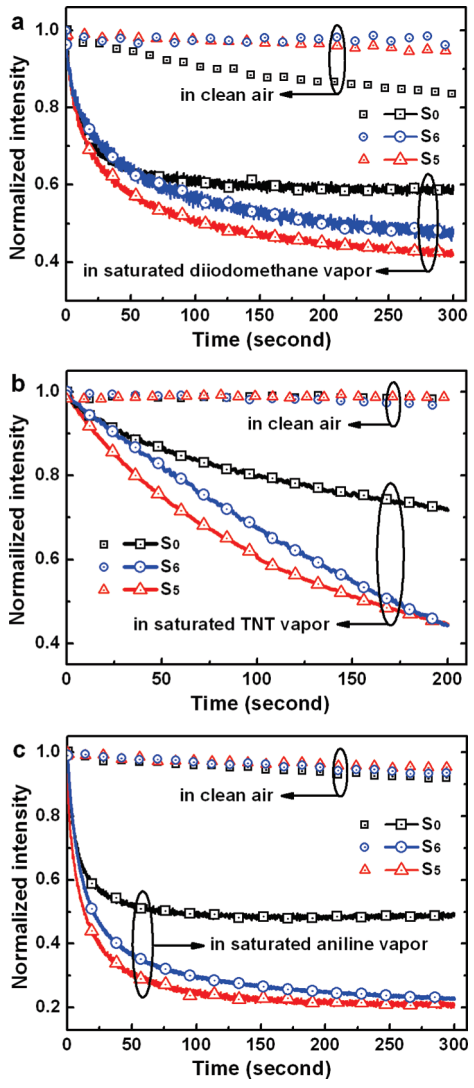

Figure 5. Sensing performance of sensors based on S_0, S_5, and S_6. Time-dependent fluorescence spectra of (a) PF-derivative-based sensors at 427 nm, (b) PPE-based sensors at 460 nm, and (c) TPA-BTD-Py-based sensors at 567 nm, when exposed to clean air or corresponding saturated vapors.

diffusion time could be neglected. Figure 5 shows the time dependence of normalized fluorescence intensity at emission peaks of the three sensing materials in clean air or upon exposure to saturated target vapors. To compare the sensing performance with reference sensors, S_5 was selected as an optical waveguide of sensors for its high uniformity and verticality, sharp enhancement in fluorescence, and large detection surface. Additionally, S_6, namely, the vertical nanorod array, was introduced into the comparison. With extended time, all sensors kept steady in clean air except the reference sensor of the PF derivative (photobleaching was 15.5%, as shown in Figure 5a). However, a different response appeared upon exposure to the target vapors.

Figure 5a displays response curves of the PF-derivative-coated sensors to saturated diiodomethane vapor. When the S_5-based sensor was used instead of the reference sensor, the normalized fluorescence quenching rate (FQR) rose from 39% to 58% in 300 s, and the full-load time lengthened from about 50 s to more than 180 s. Similar results were obtained when PPE and TPA-BTD-Py were respectively used for TNT and aniline vapor detection (Figure 5b,c). Upon exposure to the saturated TNT vapor, the normalized FQR of the S_5-based TNT sensor was about twice as large than that of the reference sensor at any moment. With regard to TPA-BTD-Py, when S_5 was introduced as the waveguide, the normalized FQR rose from 50% to 80% in 300 s and the full-load time was lengthened from less than 60 s to more than 120 s in the saturated aniline vapor. Although S_6 also displayed obviously enhanced sensing performance compared with the reference sensor for its vertical nanorod array, S_5 is an even better choice since it presented higher normalized FQRs for all three sensing events at the beginning (Figure 5). This should be attributed to the structural difference of the AFAs in S_5 of a much larger vertically projected area because of the inner cross-nanorods. As target molecules diffuse into the nanorod arrays of S_5 and S_6 from the surface, cross-nanorods in the AFAs provide more chances to combine with target molecules in a short time. Notablely, the curves in Figure 5 indicate only the normalized FQRs of different sensors; actually, the absolute intensity change for S_5 within the same time scale is far higher than that of S_6 because of its higher initial emission intensity, as discussed above.

Reasons for the sensitivity improvement of S_5-based sensors are as follows. On one hand, the ASE action of sensing materials quickly improved the sensitivity. According to the theoretical analysis of the quenching process on ASE action,[7] E_{TH} of the fluorescent material is increased in the presence of target vapor molecules and the optimal sensitivity is obtained when the excitation density is slightly above the E_{TH}.[9] In our work, the spectra were moderately narrowed, indicating that the excitation energy densities were slightly above the E_{TH} of ASE, which met the demand for sensitivity enhancement. On the other hand, ordered AFAs of ZnO nanorods formed a high-performance sensing structure. In our experiments, concentrations of vapors were very low, which means the number of vapor molecules was much smaller than fluorescence molecules in the sensors. 3D structures of the ZnO AFAs support a larger surface and more active bonding sites and take longer to completely quench the excited fluorescence molecules. Besides, as villi in a dog's nasal cavity, the assemblies in sensors provide large interspaces to store vapor molecules with a longer residence time, which could highly increase the probability of an encounter with sensing molecules and ultimately induce quick fluorescence quenching.

CONCLUSION

In summary, a 3D assembly structure of ZnO nanorods has been hydrothermally fabricated over a large area with stress control. As waveguides and substrates of fluorescence sensors, the ordered ZnO AFAs bring about ASE actions of fluorescent materials, increase the response (quenching) rate, and prolong the full-load time without exception. The evanescent-wave property of ZnO nanorods allows high density of excitation energy in the cladding region, leading to the ASE. For the ZnO AFAs, evanescent-field overlapping and coupling of the nanofiber cluster and vertical light emission from the cluster further enhance the emission intensity. The ASE action of the sensing materials and 3D structural characteristic of the ZnO AFAs enable a considerable increase in sensitivity. Our findings expand the application of the hydrothermal process and suggest a controllable method to fabricate 3D secondary structures of 1D rigid materials. The work also provides a general and effective idea to design fluorescence sensors of higher emission intensity (higher signal-to-noise ratio), larger quenching rate (higher sensitivity), and longer full-load time (longer useful life) with structural and optical modulation on a nanoscale. Although the exact effects of experimental conditions on the structure fabrication are under research, the ordered AFAs of ZnO nanorods may have potential applications ranging from solar cells and nanolasers to safety monitoring.

METHODS

Waveguide Preparation. A mixture composed of 2.2 g of zinc acetate dihydrate, 0.6 mL of monoethanolamine, and 30 mL of 2-methoxyethanol was stirred at 60 °C for 30 min, followed by spin-coating on quartz plates at 2000 rpm for 20 s. The seed layer was heated to 120 °C for 10 min without delay to decrease the fluidity and finally formed after 1 h postannealing at 400 °C in air. Quartz plates with a ZnO seed layer were then vertically inserted into the aqueous precursor solution and heated at a constant temperature of 90 °C (for 4 to 8 h) with continuous magnetic stirring to grow AFAs of ZnO nanorods. The precursor solution was composed of 0.02 mol/L zinc nitrate [$Zn(NO_3)_2$], 0.02 mol/L hexamethylenetetramine [HMT, $(CH_2)_6N_4$], and 0.4 wt % PVA, whose degree of polymerization was 1800 ± 100. Vertical ZnO nanorod arrays were grown in a similar solution system at 90 °C for 8 h, in which the aqueous solvent was replaced by a mixed solvent (ethanol/water = 1:4 v/v), and concentrations of the reagents were all reduced to 0.012 mol/L. To absolutely clean adsorbates on the surface, as prepared waveguides were rinsed with pure water twice and then cleaned in ethanol for 5 min under ultrasound. Finally, the waveguides were obtained after 1 h drying at 120 °C. XRD (Rigaku D/max 2200VPC, Japan) with a Ni-filtered Cu Kα radiation source, SEM (Hitachi S-4700, Japan), and TEM (FEI Tecnai G20, XTwin, 200 KV FEG microscope, USA) were employed to characterize the crystallinity and morphology of the as-prepared nanostructures.

Sensing Elements Preparation. For diiodomethane sensors, a PF-derivative/toluene solution (10^{-4} M) was spin coated on different kinds of substrates at 2000 rpm for 20 s and then put in a vacuum chamber at room temperature for 1 h to remove the solvent. For aniline sensors, the preparation process was the same as that for diiodomethane sensors, and the concentration of the TPA-BTD-Py/toluene solution was 10^{-4} M. For TNT sensors, the PPE/toluene solution (10^{-5} M) was spin coated on quartz plates and as prepared structures at 2000 rpm for 20 s and then heated at 60 °C for 1 h under vacuum.

Fluorescence and Response Measurement. Fluorescence responses to the three vapors were ascertained at room temperature by inserting sensors into sealed vials (20 mL size) containing test material (TNT powder or diiodomethane droplets or aniline droplets) and cotton gauze, which prevented direct sensor analyte contact and helped maintain a constant vapor pressure. The fluorescence spectra were recorded immediately after exposing the sensors to relative target vapors for a specific time. All fluorescence spectra of the samples were measured with a spectrofluorometer (Jasco FP-6500, Japan).

Acknowledgment. This work was supported by the research programs from the National Natural Science Foundation of China (Nos. 61007066, 51003118, 60977067, 50973128, and 20773156), Ministry of Science and Technology of China (Program Nos. 2007AA06A407, 2009BAK64B03), "Bairen Program" of CAS, SIMIT Technology and Innovation Foundation, and Shanghai Science and Technology Committee (Grant No. 09XD1405000).

Supporting Information Available: Structure characterization of the ZnO AFAs and the vertical ZnO nanorod array, power distribution in radial direction of the nanorod, absorption spectrum of the ZnO AFAs, and original spectra of the PF-derivative-coated sensors. This material is available free of charge *via* the Internet at http://pubs.acs.org.

REFERENCES AND NOTES

1. Wang, F.; Gu, H. W.; Swager, T. M. Carbon Nanotube/polythiophene Chemiresistive Sensors for Chemical Warfare Agents. *J. Am. Chem. Soc.* **2008**, *130*, 5392–5393.
2. Swager, T. M. The Molecular Wire Approach to Sensory Signal Amplification. *Acc. Chem. Res.* **1998**, *31*, 201–207.
3. Zhao, Y. S.; Fu, H. B.; Hu, F. Q.; Peng, A. D.; Yao, J. N. Multicolor Emission from Ordered Assemblies of Organic 1D Nanomaterials. *Adv. Mater.* **2007**, *19*, 3554–3558.
4. Levitsky, I. A.; Euler, W. B.; Tokranova, N.; Rose, A. Fluorescent Polymer-Porous Silicon Microcavity Devices for Explosive Detection. *Appl. Phys. Lett.* **2007**, *90*, 041904.
5. Uthirakumar, P.; Lee, Y. S.; Suh, E. K.; Hong, C. H. Hybrid Fluorescent Polymer–Zinc Oxide Nanoparticles: Improved Efficiency for Luminescence Conversion LED. *J. Lumin.* **2008**, *128*, 287–296.
6. Wosnick, J. H.; Liao, J. H.; Swager, T. M. Layer-by-Layer Poly(phenylene ethynylene) Films on Silica Microspheres for Enhanced Sensory Amplification. *Macromolecules* **2005**, *38*, 9287–9290.
7. Zhou, Q.; Swager, T. M. Methodology for Enhancing the Sensitivity of Fluorescent Chemosensors: Energy Migration in Conjugated Polymers. *J. Am. Chem. Soc.* **1995**, *117*, 7017–7018.
8. McQuade, D. T.; Pullen, A. E.; Swager, T. M. Conjugated Polymer-Based Sensory Materials. *Chem. Rev.* **2000**, *100*, 2537–2574.
9. Rose, A.; Zhu, Z. G.; Madigan, C. F.; Swager, T. M.; Bulovic, V. Sensitivity Gains in Chemosensing by Lasing Action in Organic Polymers. *Nature* **2005**, *434*, 876–879.
10. Tong, L. M.; Gattass, R. R.; Ashcom, J. B.; He, S. L.; Lou, J. Y.; Shen, M. Y.; Maxwell, I.; Mazur, E. Subwavelength-Diameter Silica Wires for Low-Loss Optical Wave Guiding. *Nature* **2003**, *426*, 816–819.

11. Gu, F. X.; Zhang, L.; Yin, X. F.; Tong, L. M. Polymer Single-Nanowire Optical Sensors. *Nano Lett.* **2008**, *8*, 2757–2761.
12. Laroche, M.; Albaladejo, S.; Carminati, R.; Sáenz, J. J. Optical Resonances in One-Dimensional Dielectric Nanorod Arrays: Field-Induced Fluorescence Enhancement. *Opt. Lett.* **2007**, *32*, 2762–2764.
13. Zhu, D. F.; He, Q. G.; Cao, H. M.; Cheng, J. G.; Feng, S. L.; Xu, Y. S.; Lin, T. Poly(phenylene ethynylene)-Coated Aligned ZnO Nanorod Arrays for 2,4,6-Trinitrotoluene Detection. *Appl. Phys. Lett.* **2008**, *93*, 261909.
14. Tong, L. M.; Lou, J. Y.; Mazur, E. Single-mode Guiding Properties of Subwavelength-Diameter Silica and Silicon Wire Waveguides. *Opt. Express* **2004**, *12*, 1025–1035.
15. Li, Z. Y.; Ho, K. M. Bloch Mode Reflection and Lasing Threshold in Semiconductor Nanowire Laser Arrays. *Phys. Rev. B* **2005**, *71*, 045315.
16. Crosignani, B.; Papas, C. H.; Porto, P. D. Coupled-mode Theory Approach to Nonlinear Pulse Propagation in Optical Fibers. *Opt. Lett.* **1981**, *6*, 61–63.
17. Lehmann, K. K.; Romanini, D. The Superposition Principle and Cavity Ring-Down Spectroscopy. *J. Chem. Phys.* **1996**, *105*, 10263–10277.
18. Matefi-Tempfli, S.; Matefi-Tempfli, M.; Vlad, A.; Antohe, V.; Piraux, L. Nanowires and Nanostructures Fabrication Using Template Methods: a Step Forward to Real Devices Combining Electrochemical Synthesis with Lithographic Techniques. *J. Mater. Sci.: Mater. Electron.* **2009**, *20*, S249–254.
19. Zeng, H.; Li, J.; Liu, J. P.; Wang, Z. L.; Sun, S. H. Exchange-Coupled Nanocomposite Magnets by Nanoparticle Self-Assembly. *Nature* **2002**, *420*, 395–398.
20. Gao, P. X.; Wang, Z. L. Mesoporous Polyhedral Cages and Shells Formed by Textured Self-Assembly of ZnO Nanocrystals. *J. Am. Chem. Soc.* **2003**, *125*, 11299–11305.
21. Hsu, J. W. P.; Tian, Z. R.; Simmons, N. C.; Matzke, C. M.; Voigt, J. A.; Liu, J. Directed Spatial Organization of Zinc Oxide Nanorods. *Nano Lett.* **2005**, *5*, 83–86.
22. Pokroy, B.; Kang, S. H.; Mahadevan, L.; Aizenberg, J. Self-Organization of a Mesoscale Bristle into Ordered, Hierarchical Helical Assemblies. *Science* **2009**, *323*, 237–240.
23. Zhou, X. F.; Chen, S. Y.; Zhang, D. Y.; Guo, X. F.; Ding, W. P.; Chen, Y. Microsphere Organization of Nanorods Directed by PEG Linear Polymer. *Langmuir* **2006**, *22*, 1383–1387.
24. Gautam, U. K.; Panchakarla, L. S.; Dierre, B.; Fang, X. S.; Bando, Y.; Sekiguchi, T.; Govindaraj, A.; Golberg, D.; Rao, C. N. R. Solvothermal Synthesis, Cathodoluminescence, and Field-Emission Properties of Pure and N-Doped ZnO Nanobullets. *Adv. Funct. Mater.* **2009**, *19*, 131–140.
25. Vayssieres, L. Growth of Arrayed Nanorods and Nanowires of ZnO from Aqueous Solutions. *Adv. Mater.* **2003**, *15*, 464–466.
26. Elias, J.; Claude, L.-C.; Bechelany, M.; Michler, J.; Wang, G.-Y.; Wang, Z.; Philippe, L. Hollow Urchin-like ZnO Thin Films by Electrochemical Deposition. *Adv. Mater.* **2010**, *22*, 1607–1612.
27. Wang, J.; Gudiksen, M. S.; Duan, X.; Cui, Y.; Lieber, C. M. Highly Polarized Photoluminescence and Photodetection from Single Indium Phosphide Nanowires. *Science* **2001**, *293*, 1455–1457.
28. Huang, M. H.; Mao, S.; Feick, H.; Yan, H. Q.; Wu, Y. Y.; Kind, H.; Weber, E.; Russo, R.; Yang, P. D. Room-Temperature Ultraviolet Nanowire Nanolasers. *Science* **2001**, *292*, 1897–1899.
29. Bogan, M. J.; Agnes, G. R. Poly(ethylene glycol) Doubly and Singly Cationized by Different Alkali Metal Ions: Relative Cation Affinities and Cation-Dependent Resolution in a Quadrupole Ion Trap Mass Spectrometer. *J. Am. Soc. Mass Spectrom.* **2002**, *13*, 177–186.
30. Zhang, G. Z.; Wu, C. Reentrant Coil-to-Globule-to-Coil Transition of a Single Linear Homopolymer Chain in a Water/Methanol Mixture. *Phys. Rev. Lett.* **2001**, *86*, 822–825.
31. Dev, A.; Chaudhuri, S. Uniform Large-Scale Growth of Micropatterned Arrays of ZnO Nanowires Synthesized by a Surfactant Assisted Approach. *Nanotechnology* **2007**, *18*, 175607.
32. Liu, H.; Zhai, J.; Jiang, L. Wetting and Anti-wetting on Aligned Carbon Nanotube Films. *Soft Matter* **2006**, *2*, 811–821.
33. Snyder, A. W.; Love, J. D. Waveguides with exact solutions. In *Optical Waveguide Theory*; Chapman and Hall: New York, 1983; pp 248−259.
34. McGehee, M. D.; Gupta, R.; Veenstra, S.; Miller, E. K.; Diaz-Garcia, M. A.; Heeger, A. J. Amplified Spontaneous Emission from Photopumped Films of a Conjugated Polymer. *Phys. Rev. B* **1998**, *58*, 7035–7039.
35. Choy, J.-H.; Jang, E.-S.; Won, J.-H.; Chung, J.-H.; Jang, D.-J.; Kim, Y.-W. Soft Solution Route to Directionally Grown ZnO Nanorod Arrays on Si Wafer; Room-Temperature Ultraviolet Laser. *Adv. Mater.* **2003**, *15*, 1911–1914.
36. Yang, J.-S.; Swager, T. M. Fluorescent Porous Polymer Films as TNT Chemosensors: Electronic and Structural Effects. *J. Am. Chem. Soc.* **1998**, *120*, 11864–11873.